Supplementary Information (SI) for Chemical Science.
This journal is © The Royal Society of Chemistry 2026

Supporting information for

Molecular basis for the biosynthetic divergence of anthracyclines kosinostatin and chartreusin

Ling Li Fang,[Δ,a] Chen Hao Jia,[Δ,a] Xuan Zhou,[a] Jun Ying Ma,[a] Huan Zi Guo,[a] Xiuxiu Ma,[d] Wei Bai,[a] Lang Xiang,[a] Jiapeng Zhu,*[b,c] Ren Xiang Tan,*[a,d] Yi Shuang Wang*[a]

a. Synthetic Biology Center for Chinese Medicine, School of Pharmacy, Nanjing University of Chinese Medicine, Nanjing 210023 (China).
b. Department of Hepatobiliary Surgery, The First Affiliated Hospital of Anhui Medical University, Hefei, Anhui, 230001 (China).
c. MOE Innovation Center for Basic Research in Tumor Immunotherapy, Anhui Province Key Laboratory of Tumor Immune Microenvironment and Immunotherapy, Anhui Provincial Innovation Institute for Pharmaceutical Basic Research, Hefei, Anhui, 230001 (China).
d. State Key Laboratory of Pharmaceutical Biotechnology, Institute of Functional Biomolecules, School of Life Sciences, Nanjing University 210023 (China)
*Corresponding author: Yi Shuang Wang (wangys@njucm.edu.cn); Ren Xiang Tan (rxtan@nju.edu.cn); Jiapeng Zhu (zhujiapeng@fy.ahmu.edu.cn).
Δ Contributed equally to this work.

Table of contents

General Procedures

HPLC analysis was carried out on an Agilent Technologies 1260 Infinity LC System, equipped with a DAD detector by a Proshell 120 EC-C18 (150 × 4.6 mm, 4 μm). The LC-HR/MS analysis was performed on an Agilent 6530 spectrometer with a Poroshell 120 (EC-C18 column, 4.5×50 mm, 2.7 μm). The 1D (^{1}H and ^{13}C) and 2D NMR spectra [^{1}H-^{1}H chemical shift correlation spectroscopy (^{1}H-^{1}H COSY), heteronuclear single quantum coherence (HSQC), heteronuclear multiple bond correlation (HMBC), nuclear overhauser effect correlation spectroscopy (NOESY)] were acquired either on a Bruker Avance III HD500 at 500 MHz for ^{1}H and 125 MHz for ^{13}C nuclei. PCR amplifications were performed on a Bio-Rad S1000™ Thermal Cycler using Phanta Super-Fidelity DNA Polymerase or 2×Rapid Taq Master Mix (Vazyme Co., Ltd) Polymerase. DNA Sequencing was conducted by Sangon Biotech (Shanghai) Co.,Ltd. Other chemicals, biochemical, and media components were purchased from standard commercial sources.

Construction of ChaU and KstA15 mutants and site-directed mutagenesis

The pET-28a was used as a cloning and expression vector for all enzymes described in this study. Primers for all the mutants' construction were described in Table S1. The following PCR protocol was used: (1) initial denaturation at 95 °C for 3 min, (2) 30 cycles of denaturation at 95 °C for 15 s, annealing at 50-60 °C for 15 s (depending on the Tm of the primers) and extension at 72 °C for 3 min; (3) final extension at 72 °C for 5 min. The positive-PCR products (verified by nucleic acid gel electrophoresis) were digested with Dpn I for 1 hour at 37 °C and 5 μL cooled mixture was transformed into DH5α directly and single colonies were cultured in LB containing 50 μg/mL kanamycin. All single colonies were grown overnight, plasmids were isolated and varCompetentnts harboring the correct mutations were identified by sequencing. Correctly sequenced mutated plasmids were transformed into *E. coli* BL21 (DE3) and a single colony was used for protein expression and purification.

Protein expression and purification

ChaUm1, ChaUm3 and other ChaU and KstA15 variants were produced and purified as previously described. The strain was used to inoculate LuriaBertani (LB) liquid medium (5 mL) containing kanamycin (50 μg/mL). After overnight incubation at 37 °C, the culture was used to inoculate fresh LB/K+ medium (200 mL). The cells were grown at 37 °C, 220 rpm until OD600 reached 0.6-0.8. Isopropyl-β-Dthiogalactopyranoside (IPTG, 0.125 mM) was added to induce protein expression. Cultures were grown at 16 °C for 16 h with shaking at 180 rpm. The cells were harvested by centrifugation at 6,000 rpm for 10 min and resuspended in a lysis buffer (100 mM Tris, pH 8.0, 15 mM imidazole, 300 mM NaCl, 10 % glycerol) and lysed on ice by sonication. The cell lysate was centrifuged at 12,000 rpm for 30 min. The supernatant was filtered through 0.45 μm filtrator (Merck millipore) and applied to Ni^{2+}-chelating affinity chromatography for protein purification. After verifying protein purities by SDS-PAGE, the protein was pooled and desalted by a PD10 column (GE Healthcare) with 100 mM sodium phosphate (pH 8.0) and 15% glycerol and stored at −80 °C prior to use.

Catalytic activity assay of ChaU and KstA15 variants

The ChaU/KstA15 variants-catalyzed reaction was carried out in 100 μL reaction mixture containing 100 mM phosphate buffer (pH 7.5), 50 μM substrate, 10 mM NADH, 10 μM purified recombinant protein, and 10 μM KstA16. After incubation at 37 °C for 2 hours, and then were quenched by addition of 1 volume of MeOH and centrifugation at 15,000 g for 10 min. And the supermatant was analyzed by HPLC or LC-MS.

Protein crystallization

Purified ChaU$^{F107L/T103I/T26I/N131G}$ protein was allowed to crystallize in MRC-2Drops 96-well plates by using the sitting-drop vapor-diffusion method. Briefly, ChaU$^{F107L/T103I/T26I/N131G}$ crystallized by mixing the gel filtration buffer (used for protein purification) with well solution (containing 14.4% w/v polyethylene glycol 8000, 20% v/v glycerol, 80mM MES (pH 6.5)，160mM Calcium acetate). The crystallization drops were incubated at 22 °C against the well solutions. The best plate-like crystals appeared in 24 h and reached final size after 2-3 days.

Data collection and refinement

Protein crystals were flash frozen in liquid nitrogen. The 3 X-ray dataset was collected from a single crystal at 100 K at BL18U1 of the Shanghai Synchrotron Radiation Facility. Images were processed with Mosflm. The crystals belonged to space group $P2_1$, with 4 molecules per asymmetric unit. The structure of ChaU$^{F107L/T103I/T26I/N131G}$ was solved by molecular replacement implemented in Phaser with the search model (PDB ID code 8KAA). The model generated from molecular replacement was used as the starting models for Phenix Autobuild.[1] Subsequently, the model was manually built by using COOT and refined by Phenix refinement.[2] The coordinates for the model of ChaU has been deposited in the Protein Data Bank, https://www.rcsb.org (PDB ID code 22JH).

Molecular docking

The initial docking poses of the corresponding substrates were taken from a previous study.[3] Partial atomic charges of the two substrates were calculated using *ab initio* quantum chemical calculations performed with ORCA 6.0.[4] Electrostatic potential calculations were carried out at the Hartree–Fock level with the 6-31G* basis set. The resulting electrostatic potentials were subsequently used to derive RESP charges using Multiwfn package.[5]

Topology and force field parameters for the substrates were generated with ACPYPE based on the GAFF2.[6-7] The protein was described using the AMBER14 force field.[8] Each protein–substrate complex was then placed in a dodecahedral simulation box, with a minimum distance of 1.0 nm between any solute atom and the box boundary. The systems were solvated with the TIP3P water model,[9] and 0.1 M NaCl was added to reproduce the experimental ionic strength.

Molecular dynamics simulations

Energy minimization was carried out using the steepest descent algorithm until convergence. This was followed by equilibration in two phases: a 1 ns NVT equilibration at 310 K, and a 1 ns NPT equilibration at 310 K and 1 bar, during which position restraints were applied to the molecule and the lipid P head.

All production MD simulations were performed using GROMACS version 2021.4 with the leap-frog integrator and a time step of 2 fs.[10] Simulations were run for a total of 250 million steps, corresponding to 500 ns. All bonds involving hydrogen atoms were constrained using the LINCS algorithm with fourth-order expansion and one iteration. Neighbor searching was performed with a grid-based scheme using a 1.4 nm cutoff for both electrostatic and van der Waals interactions. Long-range electrostatics were treated with the Particle Mesh Ewald (PME) method.[11]

Temperature coupling was applied separately to the protein and the solvent using the velocity-rescale thermostat with a time constant of 2 ps and reference temperature of 310 K.[12] Pressure was maintained at 1 bar using the Parrinello–Rahman barostat with isotropic coupling, a coupling constant of 2 ps, and a compressibility of 4.5×10^{-5} bar^{-1}.[13] The simulation box was scaled based on the center-of-mass. Periodic boundary conditions were applied in all directions, and long-range dispersion corrections were applied to both energy and pressure.

Table S1. Primers used in this study.

Primers	Sequence (5' to 3')
ChaU-D15A-F	ATGGTCgctGCATGGAATCGCGGGGAGCTCGG
ChaU-D15A-R	TTCCATGCagcGACCATCTCGAGACAGCGTTTC
ChaU-G20W-F	TGGAATCGCtggGAGCTCGGCGGAGTCACGGC
ChaU-G20W-R	AGCTCccaGCGATTCCATGCAGCGACCATCTC
ChaU-T26I-F	AGTCattGCGCACTGGTCACCGGACGTCGTCC
ChaU-T26I-R	ACCAGTGCGCaatGACTCCGCCGAGCTCCCAG
ChaU-H36Y-F	CGTCCATtatTCCGAGGAAAGGATCGTGCCGA
ChaU-H36Y-R	CCTCGGAataATGGACGACGTCCGGTGACCAG
ChaU-E39D-F	TTCCGAGgatAGGATCGTGCCGAACGAGGAAA
ChaU-E39D-R	CGATCCTatcCTCGGAATAATGGACGACGTCC
ChaU-L49R-F	AAATGGTCcgtCGCATGGAATCCGGCCTGACG
ChaU-L49R-R	CATGCGacgGACCATTTCCTCGTTCGGCACGA
ChaU-T98K-F	GAACCGGaaaGTGACCTGGCACACTGCGGAGG
ChaU-T98K-R	AGGTCACtttCCGGTTCGTCGGAGCGATGTCC
ChaU-A104V-F	GCACACTgttGAGGAGCTTCGCTTCGTCGACG
ChaU-A104V-R	GCTCCTCaacAGTGTGCCAGGTCACTTTCCGG
ChaU-F107L-F	TTGAGGAGcttCGCTTCGTCGACGGCAAGGTC
ChaU-F107L-R	GAAGCGaagCTCCTCAACAGTGTGCCAGGTCA
ChaU-N131G-F	GGAGTTGggtATGGTCGGCTCCGACGTGCGCG
ChaU-N131G-R	CGACCATaccCAACTCCCGCAGCATCGGCATG
ChaU-G134P-F	TTGGGTATGGTCcctTCCGACGTGCGCGGCTGG
ChaU-G134P-R	GAaggGACCATACCCAACTCCCGCAGCATCGG
ChaUm1-S135A-F	ATGGTCCCTgctGACGTGCGCGGCTGGGGAAC
ChaUm1-S135A-R	ACGTCagcAGGGACCATACCCAACTCCCGCAG
ChaUm1-M124L-F	CAACTACcttCCGATGCTGCGGGAGTTGGGTA
ChaUm1-M124L-R	GCATCGGaagGTAGTTGATGACATCCCAGTGCTC
ChaUm1-T103I-F	CTGGCACattGTTGAGGAGCTTCGCTTCGTCG
ChaUm1-T103I-R	CCTCAACaatGTGCCAGGTCACTTTCCGGTTC
ChaUm1-T100A-F	GAAAGTGgctTGGCACATTGTTGAGGAGCTTC
ChaUm1-T100A-R	TGTGCCAagcCACTTTCCGGTTCGTCGGAGCG
ChaUm3-I103T-F	TTGGCACactGTTGAGGAGCTTCGCTTCGTCG
ChaUm3-I103T-R	CCTCAACagtGTGCCAAGCCACTTTCCGGTTC
ChaUm3-L107F-F	TGAGGAGtttCGCTTCGTCGACGGCAAGGTCG
ChaUm3-L107F-R	CGAAGCGaaaCTCCTCAACAATGTGCCAAGCC
KstA15-I117T-F	GTGGCACactGTTGAAGAACTGCGTTTCGTTG
KstA15-I117T-R	CTTCAACagtGTGCCACGCAACTTTACGGTTG
KstA15-L121F-F	tttCGTTTCGTTGATGGCAAAGTTGTTGAACA
KstA15-L121F-R	CCATCAACGAAACGaaaTTCTTCAACGATGTGCCACG
KstA15-I40T-F	TCactAAATACTGGGCGCCGGATGTTGTTCAC
KstA15-I40T-R	CGCCCAGTATTTagtGATACCATCCAGTTCCCAACGG
KstA15-G145N-F	CTGaatAAAGTTCCGGCAGATGTGAAGCTTGC
KstA15-G145N-R	GCCGGAACTTTattCAGTTCTTTCAGCATCGGCAG

KstA15-S51A-F	GTTCACTACgctGAAGATAAAGTTGTTGATACCGATGAA
KstA15-S51A-R	TCTTCagcGTAGTGAACAACATCCGGCGCCCA
KstA15-E52A-F	GTTCACTACTCTgctGATAAAGTTGTTGATACCGATGAAATG
KstA15-E52A-R	TCagcAGAGTAGTGAACAACATCCGGCGCCCA
KstA15-R64A-F	GATCCGTgctATGGAAGGCGGCATCCAGGCGT
KstA15-R64A-R	CTTCCATagcACGGATCATTTCATCGGTATCAA
KstA15-D133A-F	ACACTGGgctGTTATGAACTACCTGCCGATGCT
KstA15-D133A-R	TCATAACagcCCAGTGTTCAACAACTTTGCCA
$ChaU^{F107L/T103I/T26I/N131G}$-H117A-F	GAGgctTGGGATGTCATCAACTACATGCCGAT
$ChaU^{F107L/T103I/T26I/N131G}$-H117A-R	ATGACATCCCAagcCTCGACGACCTTGCCGTCG
$ChaU^{F107L/T103I/T26I/N131G}$-E105A-F	ACATTGCGgctGAGCTTCGCTTCGTCGACGGC
$ChaU^{F107L/T103I/T26I/N131G}$-E105A-R	AAGCTCagcCGCAATGTGCCAGGTCACCGTCC

Table S2. The plasmids used in this study.

Plasmids	Description	Source
pET28a(+)	Protein co-expression vector used in *E. coli*, encoding N-terminal 6×His tag, Kan^r	Invitrogen
pYW00016	pET28a-derived plasmid harboring *ChaUm1* gene cloned into *Nde*I/*Hind*III sites	This study
pYW00017	pET28a-derived plasmid harboring *ChaUm2* gene cloned into *Nde*I/*Hind*III sites	This study
pYW00018	pET28a-derived plasmid harboring *ChaUm3* gene cloned into *Nde*I/*Hind*III sites	This study
pYW00019	pET28a-derived plasmid harboring *ChaUm3*^{I103T} gene cloned into *Nde*I/*Hind*III sites	This study
pYW00020	pET28a-derived plasmid harboring *ChaUm3*^{L103F} gene cloned into *Nde*I/*Hind*III sites	This study
pYW00021	pET28a-derived plasmid harboring *ChaU*^{F107L} gene cloned into *Nde*I/*Hind*III sites	This study
pYW00022	pET28a-derived plasmid harboring *ChaU*^{T103I} gene cloned into *Nde*I/*Hind*III sites	This study
pYW00023	pET28a-derived plasmid harboring *ChaU*$^{F107L/T103I}$ gene cloned into *Nde*I/*Hind*III sites	This study
pYW00024	pET28a-derived plasmid harboring *ChaU*$^{F107L/T103I/T26I}$ gene cloned into *Nde*I/*Hind*III sites	This study
pYW00025	pET28a-derived plasmid harboring *ChaU*$^{F107L/T103I/T26I/N131G}$ gene cloned into *Nde*I/*Hind*III sites	This study
pYW00026	pET28a-derived plasmid harboring *KstA15*^{I117T} gene cloned into *Nde*I/*Hind*III sites	This study
pYW00027	pET28a-derived plasmid harboring *KstA15*^{L121F} gene cloned into *Nde*I/*Hind*III sites	This study
pYW00028	pET28a-derived plasmid harboring *KstA15*^{I40T} gene cloned into *Nde*I/*Hind*III sites	This study
pYW00029	pET28a-derived plasmid harboring *KstA15*^{G145N} gene cloned into *Nde*I/*Hind*III sites	This study
pYW00030	pET28a-derived plasmid harboring *KstA15*^{S51A} gene cloned into *Nde*I/*Hind*III sites	This study
pYW00031	pET28a-derived plasmid harboring *KstA15*^{E52A} gene cloned into *Nde*I/*Hind*III sites	This study
pYW00032	pET28a-derived plasmid harboring *KstA15*^{R64A} gene cloned into *Nde*I/*Hind*III sites	This study
pYW00033	pET28a-derived plasmid harboring *KstA15*^{D133A} gene cloned into *Nde*I/*Hind*III sites	This study
pYW00034	pET28a-derived plasmid harboring *ChaU*$^{F107L/T103I/T26I/N131G/H117A}$ gene cloned into *Nde*I/*Hind*III sites	This study
pYW00035	pET28a-derived plasmid harboring *ChaU*$^{F107L/T103I/T26I/N131G/E105A}$ gene cloned into *Nde*I/*Hind*III sites	This study

Table S3. The strains used in this study.

Strains	Description	Source
DH5α	host strain for gene cloning	Sangon Biotech (Shanghai, China)
BL21(DE3)	host strain for protein expression	Sangon Biotech (Shanghai, China)
YW00018	BL21 strain harboring pET-28a/*ChaUm1*	This study
YW00019	BL21 strain harboring pET-28a/*ChaUm2*	This study
YW00020	BL21 strain harboring pET-28a/*ChaUm3*	This study
YW00021	BL21 strain harboring pET-28a/*ChaUm3*^{I103T}	This study
YW00022	BL21 strain harboring pET-28a/*ChaUm3*^{L103F}	This study
YW00023	BL21 strain harboring pET-28a/*ChaU*^{F107L}	This study
YW00024	BL21 strain harboring pET-28a/*ChaU*^{T103I}	This study
YW00025	BL21 strain harboring pET-28a/*ChaU*$^{F107L/T103I}$	This study
YW00026	BL21 strain harboring pET-28a/ChaU$^{F107L/T103I/T26I}$	This study
YW00027	BL21 strain harboring pET-28a/*ChaU*$^{F107L/T103I/T26I/N131G}$	This study
YW00028	BL21 strain harboring pET-28a/*KstA15*^{I117T}	This study
YW00029	BL21 strain harboring pET-28a/*KstA15*^{L121F}	This study
YW00030	BL21 strain harboring pET-28a/*KstA15*^{I40T}	This study
YW00031	BL21 strain harboring pET-28a/*KstA15*^{G145N}	This study
YW00032	BL21 strain harboring pET-28a/*KstA15*^{S51A}	This study
YW00033	BL21 strain harboring pET-28a/*KstA15*^{E52A}	This study
YW00034	BL21 strain harboring pET-28a/*KstA15*^{R64A}	This study
YW00035	BL21 strain harboring pET-28a/*KstA15*^{D133A}	This study
YW00036	BL21 strain harboring pET-28a/*ChaU*$^{F107L/T103I/T26I/N131G/H117A}$	This study
YW00037	BL21 strain harboring pET-28a/*ChaU*$^{F107L/T103I/T26I/N131G/E105A}$	This study

Table S4. Data collection and refinement statistics of ChaU$^{F107L/T103I/T26I/N131G}$.

	ChaU$^{F107L/T103I/T26I/N131G}$
Data collection	
Space group	P 1 2_1 1
Cell dimensions	
a,b,c(Å)	30.76, 94.73, 102.38
α,β,γ (°)	90.00, 90.00, 90.00
Resolution (Å)	69.49-2.22 (2.34-2.22)
R_{merge} (%)	0.304 (2.582)
I/ σI	3.0 (0.9)
Completeness (%)	100
Redundancy	5.0 (4.9)
Refinement	
Resolution (Å)	19.96-2.70 (2.79-2.70)
No. reflections	31495
R_{work} / R_{free} (%)	27.19/31.36
No. atoms	8584
Protein	8584
B-factors	25.12
ligand/ion	
Water	59.37
R.ms. deviations	
Bond lengths (Å)	0.004
Bond angles (°)	0.763

Table S5. ^{1}H NMR (500 MHz) data of 8-hydroxyauramycinone (**1**) in $CDCl_3$.

position	δ_H (mult, *J*, Hz)
2	4.01 s
4	7.63 s
8-OH	12.71 s
9	7.26 d (8.6)
10	7.24 d (8.6)
11-OH	12.05 s
15-OH	12.84 s
17	5.35 d (4.0)
17-OH	4.20 s
18	2.23 d (14.9), 2.61 dd (5.2, 14.9)
19-OH	3.59 s
20	1.43 s
21	3.72 s

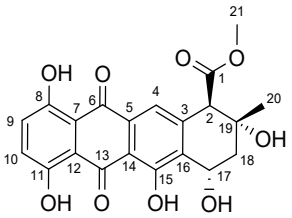

Table S6. ^{1}H NMR (500 MHz) data of resomycin C (**2**) in $CDCl_3$.

position	δ_H (mult, *J*, Hz)
4	8.28 s
8	7.94 dd (7.6, 1.2)
9	7.72 t (7.6)
10	7.34 dd (7.6, 1.2)
11-OH	13.78 s
15-OH	12.27 s
17	8.52 d (8.4)
18	7.57 d (8.4)
20	2.59 s
21	4.14 s

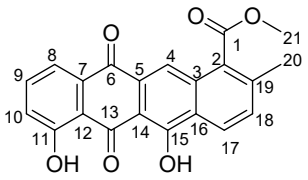

Table S7. ^{1}H NMR (500 MHz) data of auramycinone (**3**) in $CDCl_3$.

position	δ_H (mult, *J*, Hz)
2	4.06 br s
4	7.70 br s
8	7.85 br d (7.4)
9	7.70 overlapped
10	7.32 br d (7.4)
11-OH	11.96 s
15-OH	12.75 s
17	5.38 br d (4.3)
17-OH	3.37 br s
18	2.62 dd (6.2, 15.0), 2.23 d (15.0)
19-OH	4.04 br s
20	1.42 br s
21	3.72 s

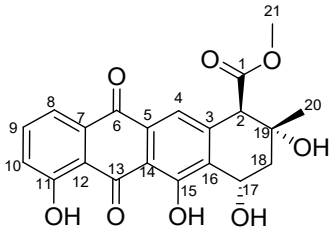

Table S8. ^{1}H NMR (500 MHz) data of **4** in acetone-d_6.

position	δ_H (mult, *J*, Hz)
4	7.59 s
8	7.78 d (7.3)
9	7.83 dd (7.3, 8.2)
10	7.35 d (8.2)
11-OH	12.03 s
15-OH	12.42 s
17	5.27 t (3.3)
18	2.73 d (3.3)
20	2.10 s
21	3.94 s

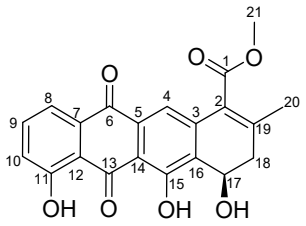

Table S9. ^{1}H NMR (500 MHz) data of **5** in $CDCl_3$.

position	δ_H (mult, *J*, Hz)
2	3.91 s
4	7.64 s
8	7.82 dd (1.1, 7.7)
9	7.68 dd (7.7, 8.2)
10	7.29 dd (1.1, 8.2)
11-OH	12.10 s
15-OH	12.51 s
17	2.88 m, 3.05 m
18	1.92 m, 2.32 m
20	1.42 s
21	3.75 s

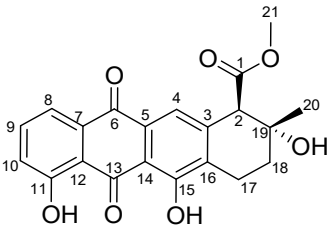

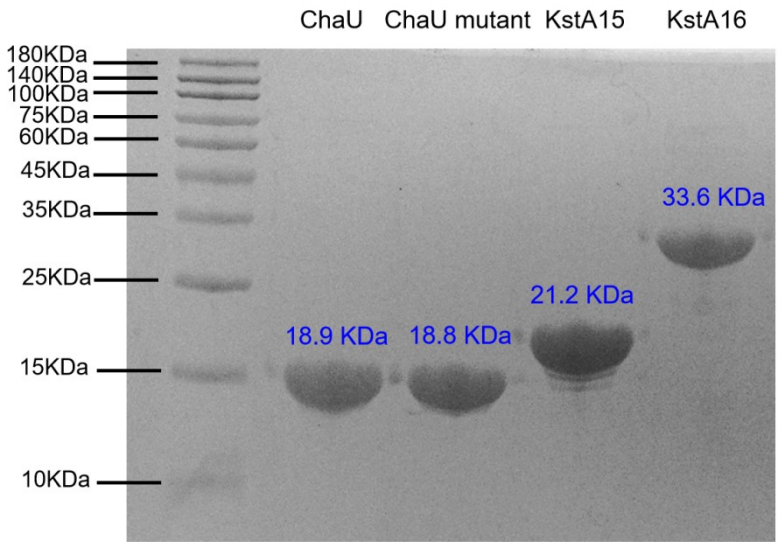

Figure S1. SDS-PAGE analysis of protein ChaU, ChaU mutant, KstA15 and KstA16. The His_6-tags in all proteins were retained. ChaU mutant here specifically refers to the $ChaU^{F107L/T103I/T26I/N131G}$ mutant.

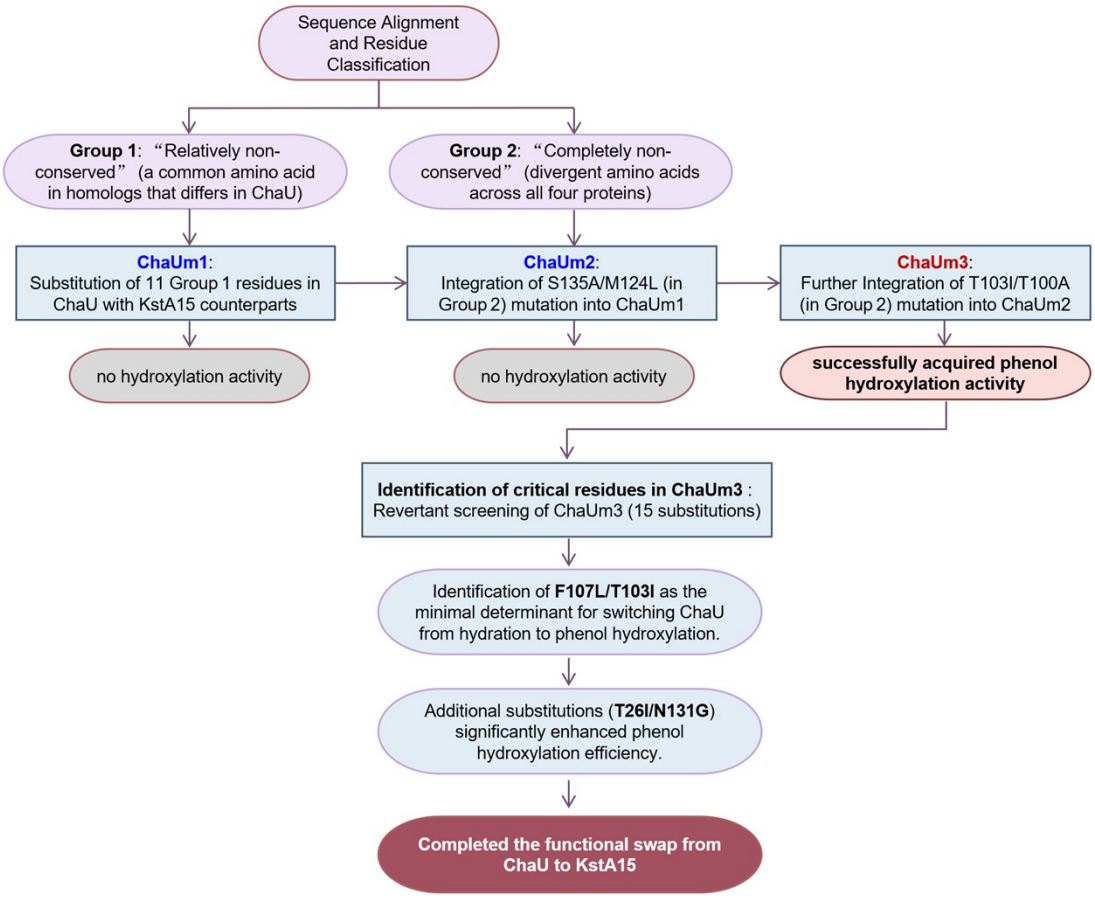

Figure S2. The schematic diagram depicting the directed evolution of ChaU.

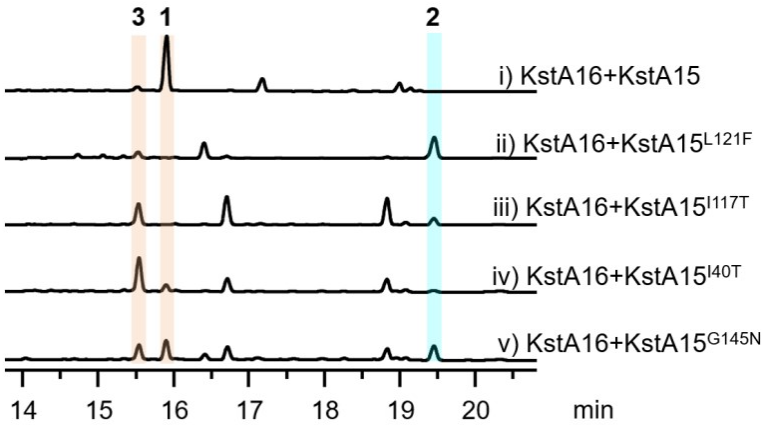

Figure S3. HPLC profiles of biochemical reactions catalyzed by KstA16 and KstA15 mutants. All assays were performed using **3** as the substrate and NADH as the cofactor, with a reaction duration of 2 hours. UV= 440 nm.

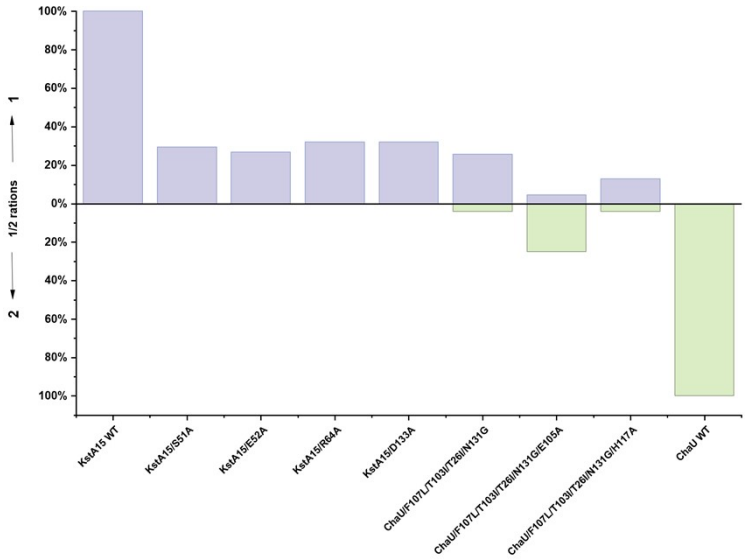

Figure S4. Comparison for enzymatic conversion rates of **3** by KstA16 and KstA15/ChaU mutants in the presence of NADH.

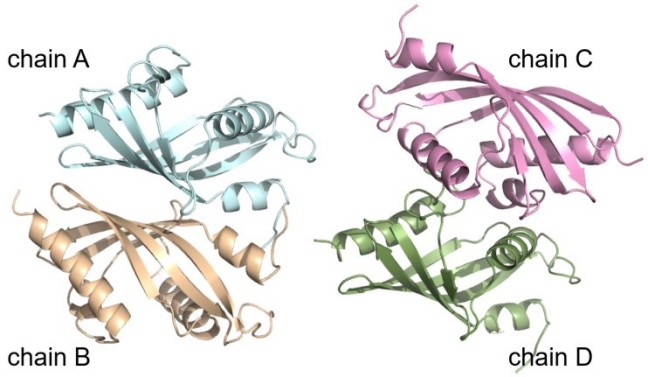

Figure S5. The tetrameric crystal structure of the ChaU$^{F107L/T103I/T26I/N131G}$ mutant (PDB: 22JH).

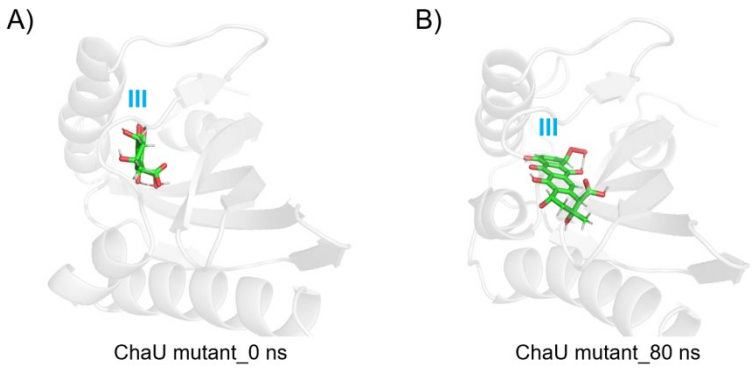

Figure S6. MD simulation snapshots showing the binding conformation of substrate **III** in the ChaU mutant at 0 ns (A) and 80 ns (B). ChaU mutant here specifically refers to the ChaU$^{F107L/T103I/T26I/N131G}$ mutant.

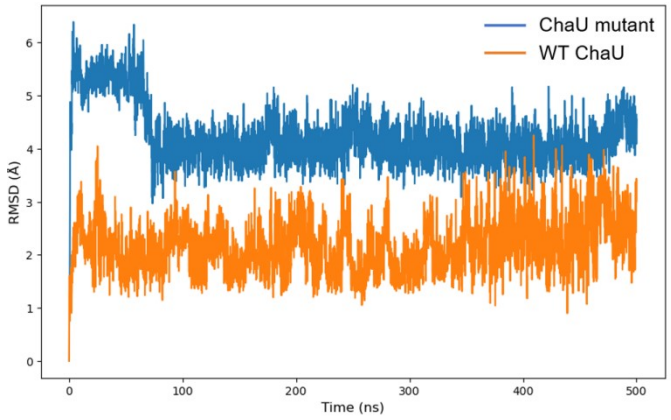

Figure S7. RMSD of backbone heavy atoms relative to the first snapshot during in the last 500 ns classical MD simulations on ChaU-**IV** complex and ChaU mutant-**III** complex. Distances are shown in Å. ChaU mutant here specifically refers to the ChaU$^{F107L/T103I/T26I/N131G}$ mutant.

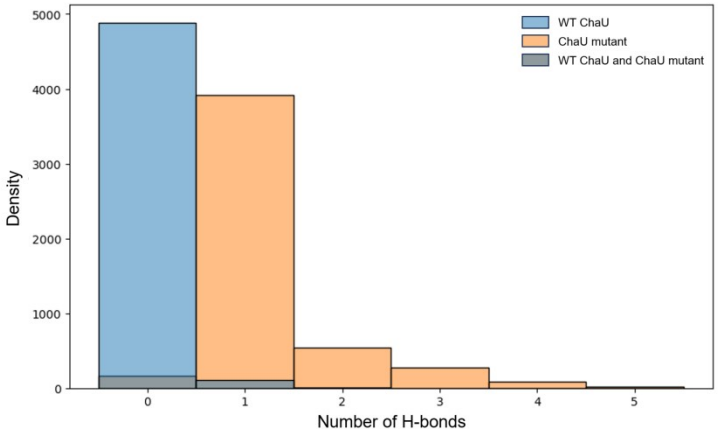

Figure S8. Distribution of H-bonds between ligand and H35/E105/H117/D119 in WT ChaU and ChaU mutant. ChaU mutant here specifically refers to the ChaU$^{F107L/T103I/T26I/N131G}$ mutant.

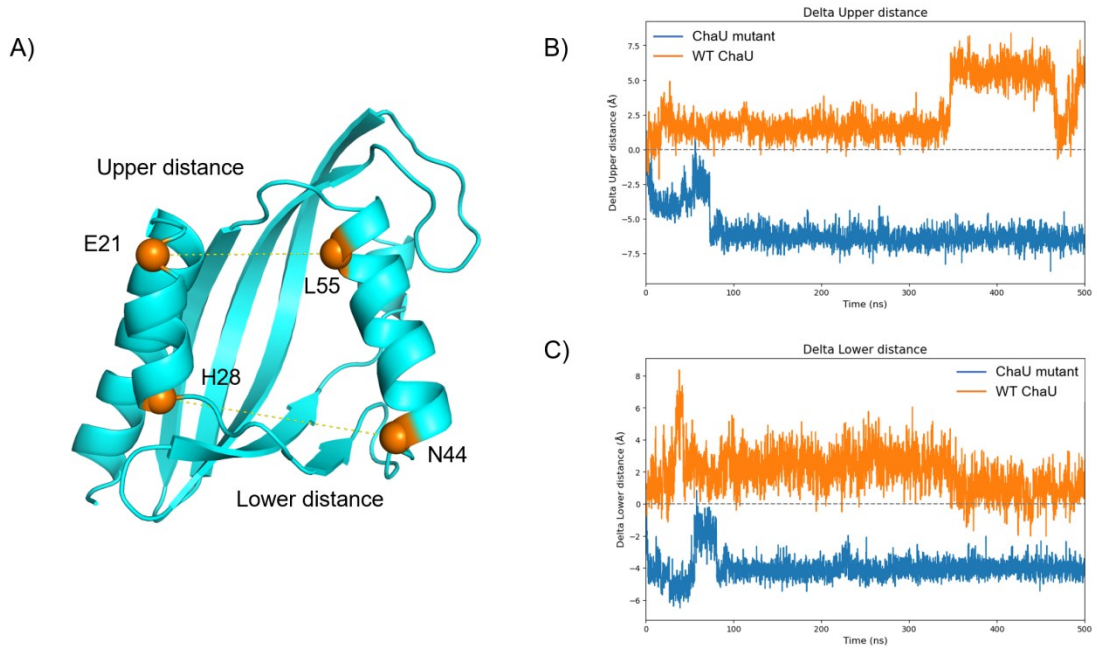

Figure S9. Deviation of the Upper and Lower distances in the MD trajectory from the corresponding distances in the crystal structure. (A) The four sites selected for measuring the Upper and Lower distances. (B-C) Comparison of Upper distances (B) and Lower distances (C) in MD trajectory and crystal structure. A positive deviation indicates that the distance is elongated in the simulation relative to the crystal structure, whereas a negative deviation signifies contraction.

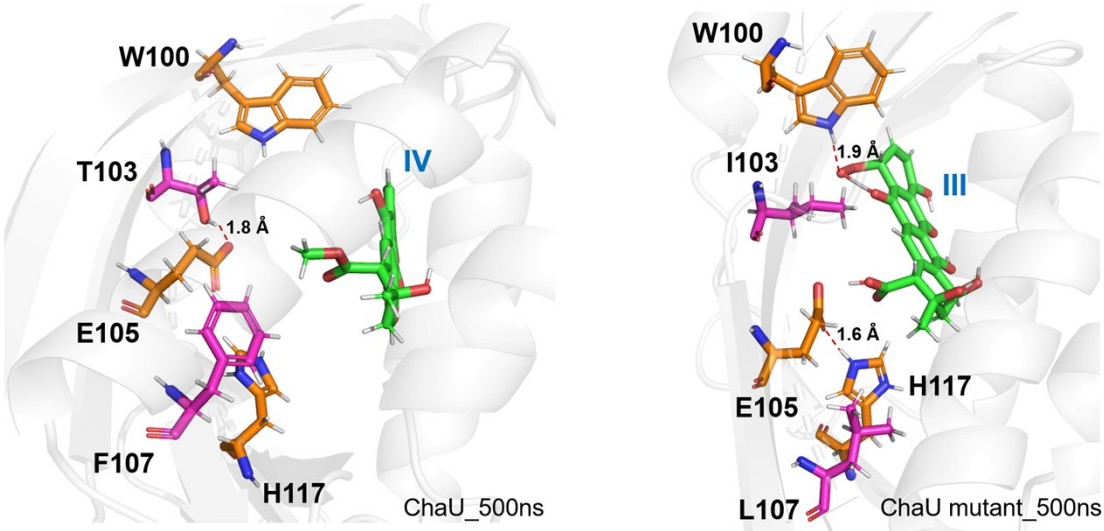

Figure S10. A comparative analysis of the interactions involving residues 100, 103, 105, and 107 (both mutual and with the substrate) in wild-type ChaU versus the ChaU mutant. Both analyses were conducted employing 500 ns MD simulations. ChaU mutant here specifically refers to the ChaU$^{F107L/T103I/T26I/N131G}$ mutant.

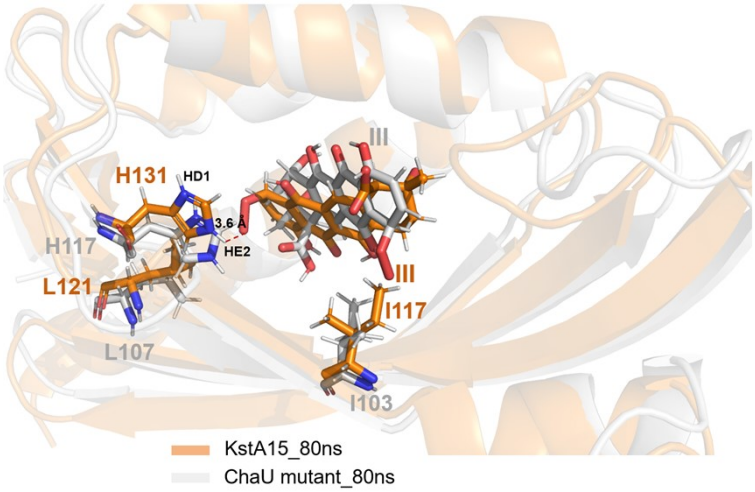

Figure S11. Comparative analysis of protein-substrate binding conformations in KstA15 and ChaU mutant. ChaU mutant here specifically refers to the ChaU$^{F107L/T103I/T26I/N131G}$ mutant. The labels HD1 and HE2 refer to the protons attached to the two nitrogen atoms in the imidazole ring of histidine.

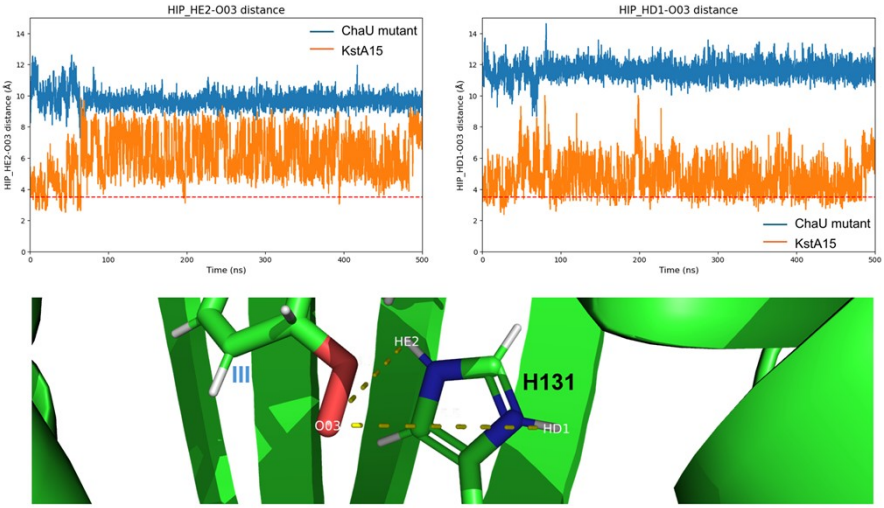

Figure S12. Comparison of the distances from HE2/HD1 of H131 to peroxide anion in MD trajectory of ChaU mutant and KstA15. ChaU mutant here specifically refers to the ChaU$^{F107L/T103I/T26I/N131G}$ mutant.

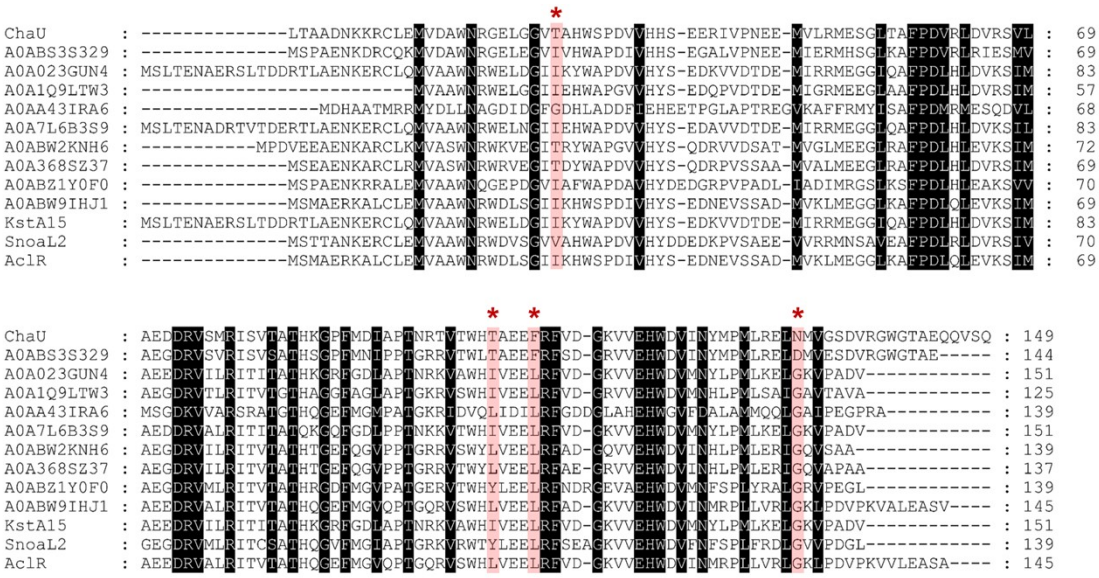

Figure S13. Alignment of ChaU, KstA15, AclR, and SnoaL2 with their homologs.

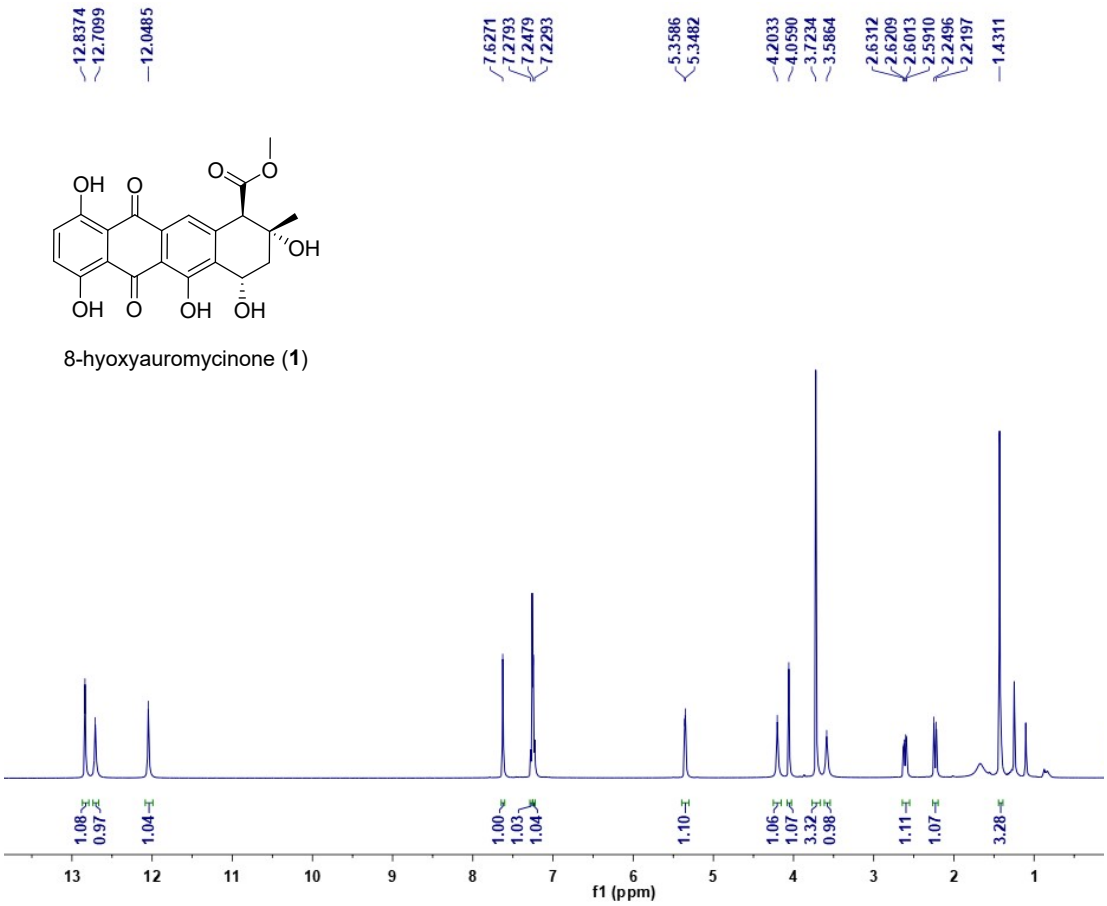

8-hyoxyauromycinone (**1**)

Figure S14. ^{1}H NMR spectrum of **1** in $CDCl_3$.

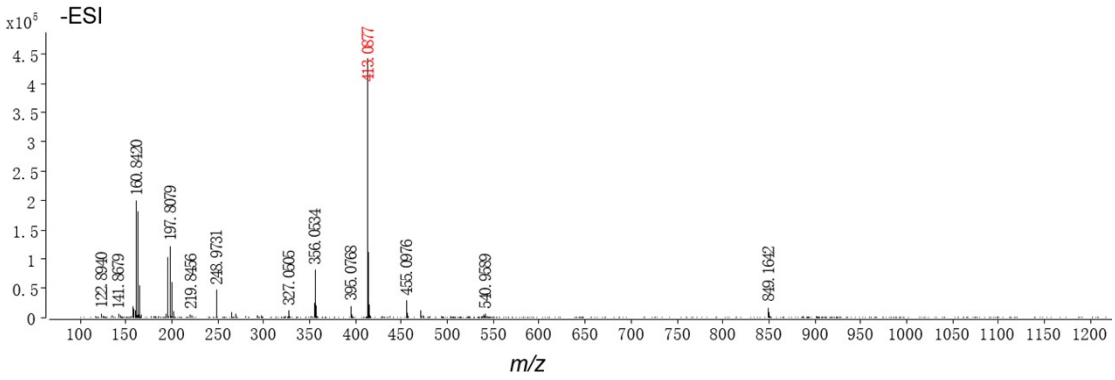

Figure S15. HR-ESIMS spectrum of **1**.

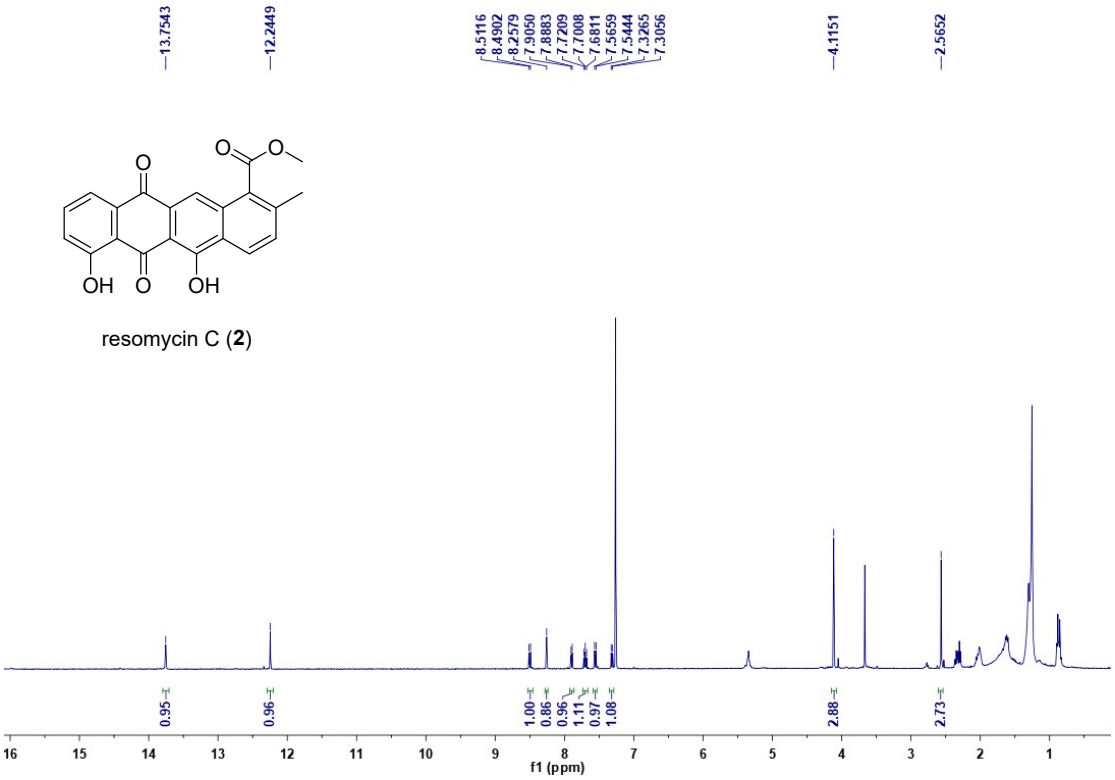

Figure S16. ^{1}H NMR spectrum of **2** in $CDCl_3$.

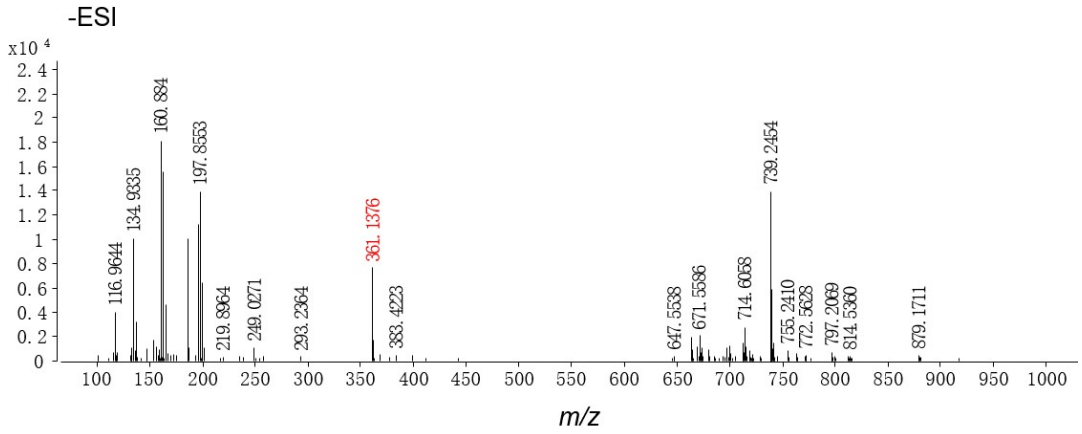

Figure S17. HR-ESIMS spectrum of **2**.

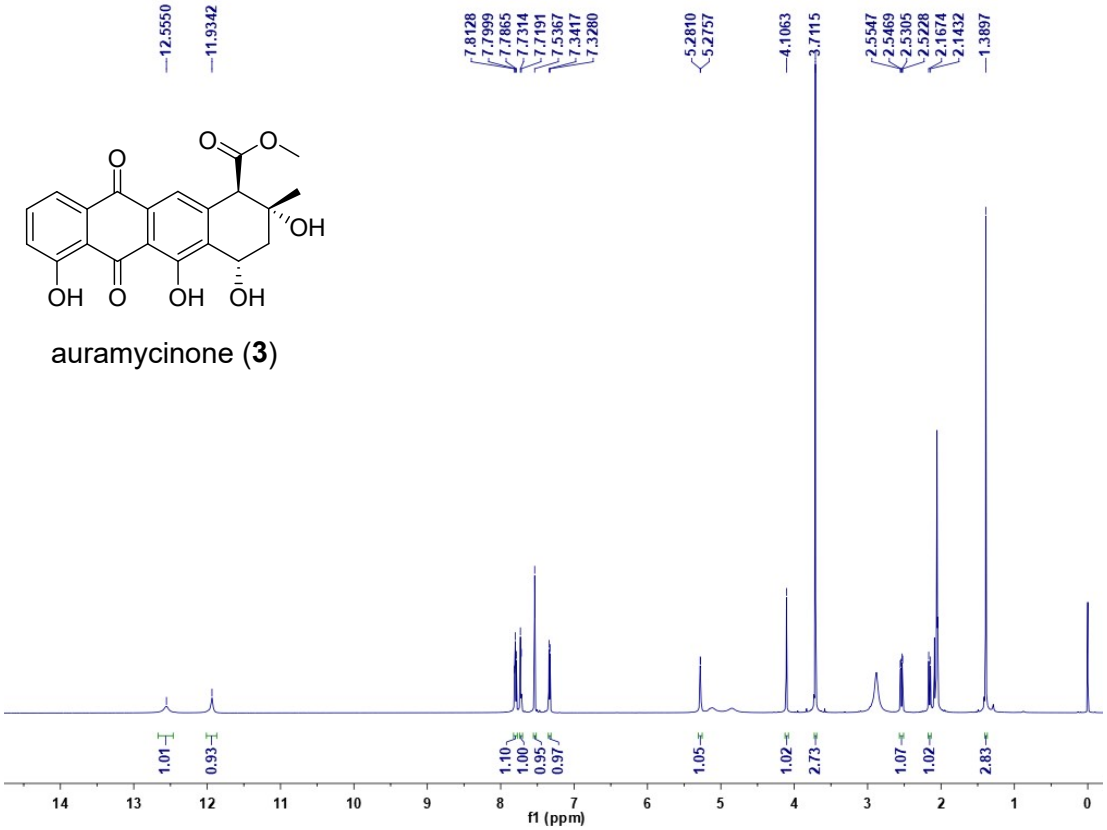

Figure S18. ^{1}H NMR spectrum of **3** in acetone-d_6.

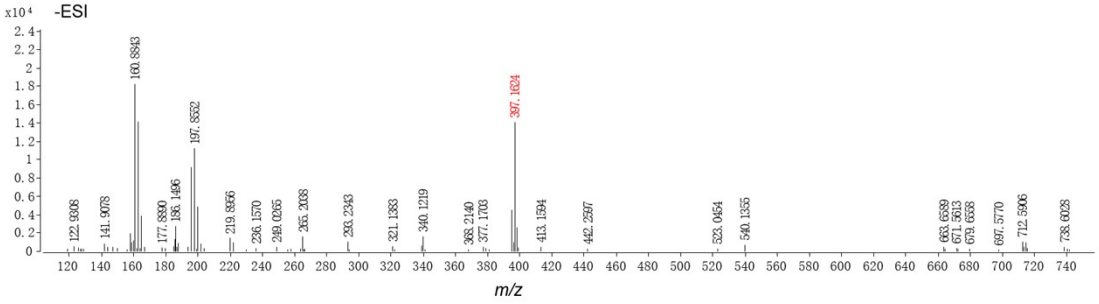

Figure S19. HR-ESIMS spectrum of **3**.

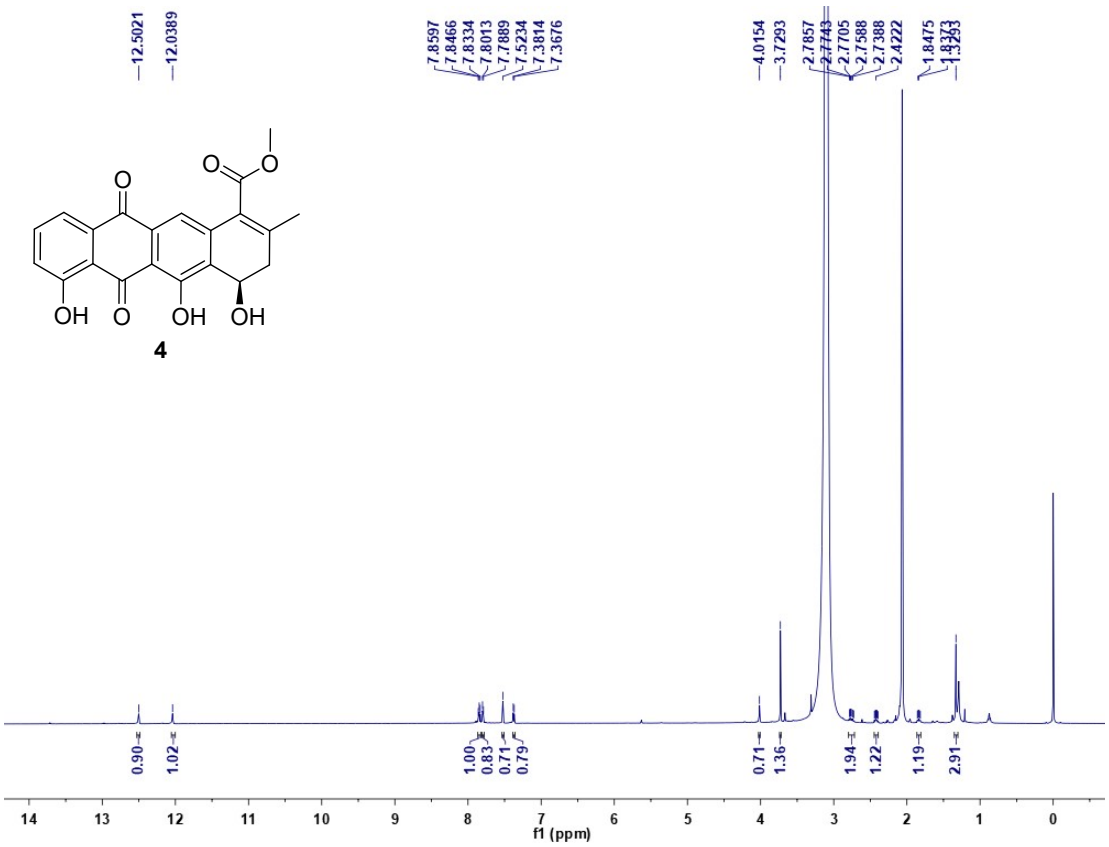

Figure S20. ^{1}H NMR spectrum of **4** in acetone-d_6.

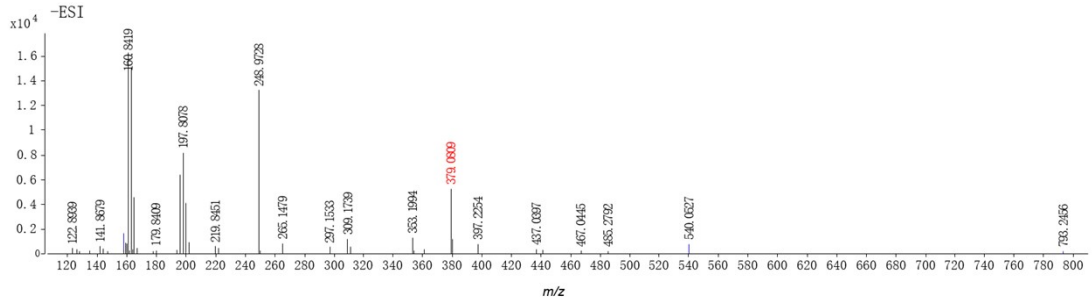

Figure S21. HR-ESIMS spectrum of **4**.

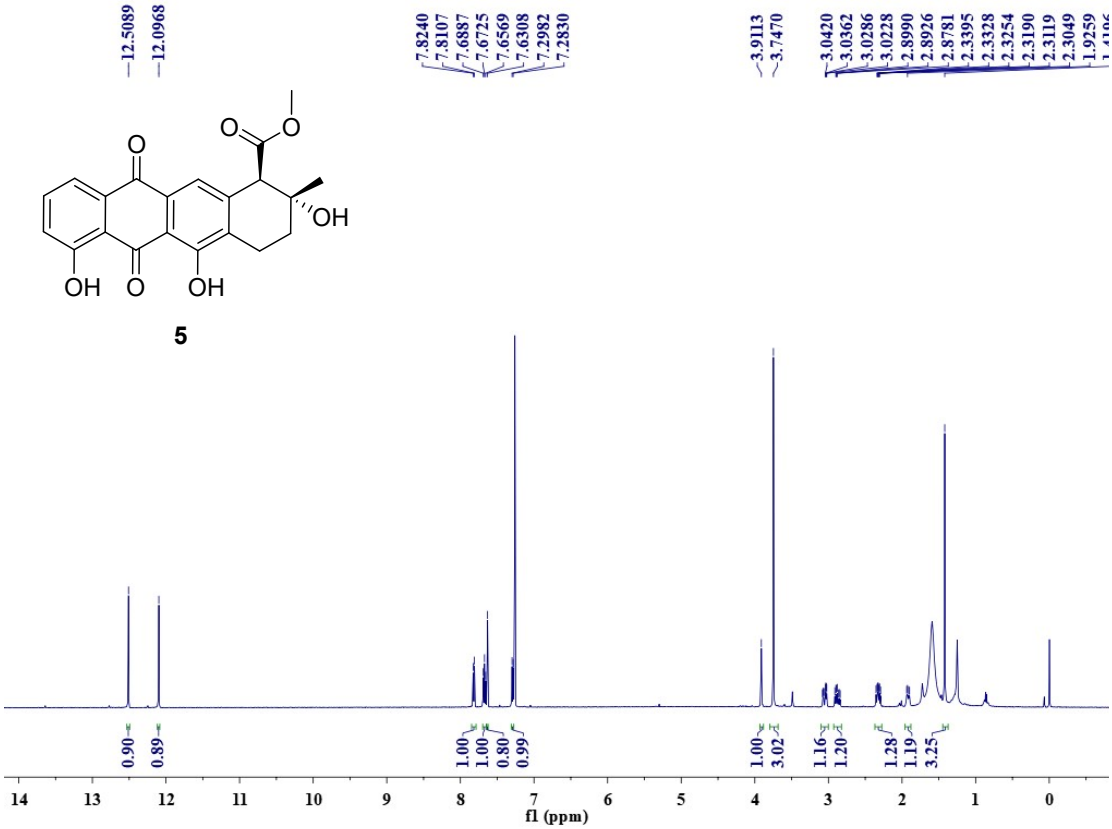

Figure S22. ^{1}H NMR spectrum of **5** in $CDCl_3$.

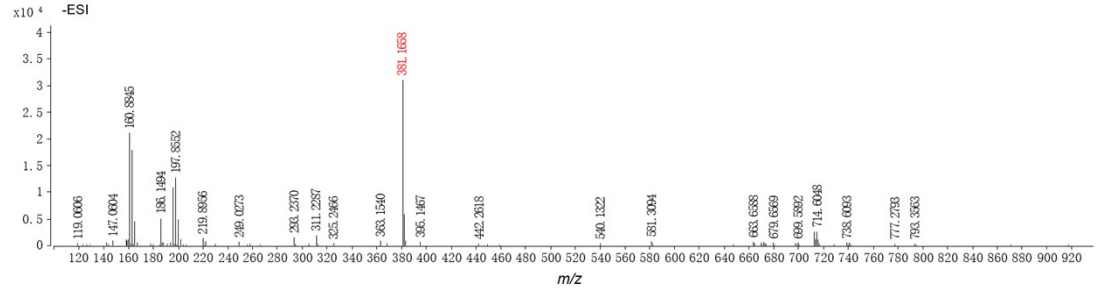

Figure S23. HR-ESIMS spectrum of **5**.

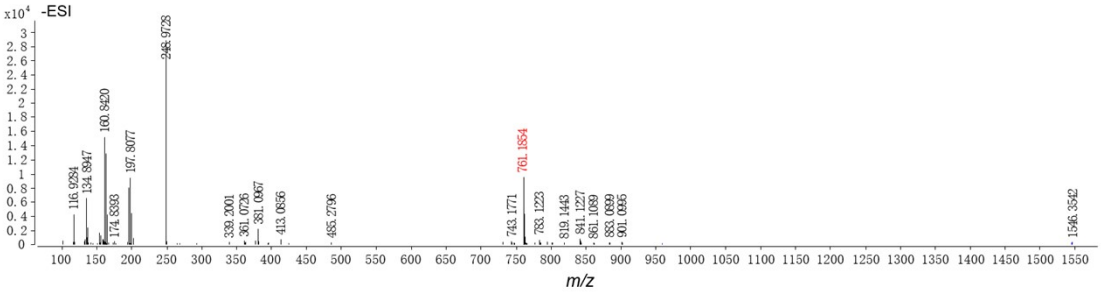

Figure S24. HR-ESIMS spectrum of **6**.

References

[1] Adams, P. D.; Afonine, P. V.; Bunkoczi, G.; Chen, V. B.; Davis, I. W.; Echols, N.; Headd, J. J.; Hung, L. W.; Kapral, G. J.; Grosse-Kunstleve, R. W.; McCoy, A. J.; Moriarty, N. W.; Oeffner, R.; Read, R. J.; Richardson, D. C.; Richardson, J. S.; Terwilliger, T. C.; Zwart, P. H. PHENIX: a comprehensive Python-based system for macromolecular structure solution. *Acta. Crystallogr. D. Biol. Crystallogr.* **2010**, *66*, 213-221.

[2] Emsley, P.; Lohkamp, B.; Scott, W. G.; Cowtan, K. Features and development of Coot. *Acta. Crystallogr. D. Biol. Crystallogr.* **2010**, *66*, 486-501.

[3] Y. S. Wang, H. W. Chen, Z. K. Meng, C. H. Jia, J. Q. Han, Y. X. Jin, X. X. Ma, N. X. Wang, J. P. Zhu, Y. Liang, and R. X. Tan, Multienzyme-Mediated Atypical Mode of Dehydration in Anthracycline Biosynthesis. *ACS Catalysis.* 2025 **15**, 19253-19267.

[4] F. Neese. Software update: The ORCA program system—version 6.0. *Wiley Interdisciplinary Reviews: Computational Molecular Science.* 2025**, 15**, e70019.

[5] T. Lu, F. Chen. Multiwfn: A multifunctional wavefunction analyzer. *Journal of computational chemistry.* 2012, **33**, 580-92.

[6] A. W. S. D. Silva, W. F. Vranken. ACPYPE-Antechamber python parser interface. *BMC research notes.* 2012, **5**, 367.

[7] X. He, V. H. Man, W. Yang, T. S. Lee, J. Wang. A fast and high-quality charge model for the next generation general AMBER force field. *The Journal of chemical physics.* 2020, **153**, 114502.

[8] J. A. Maier, C. Martinez, K. Kasavajhala, L. Wickstrom, K. E. Hauser, C. Simmerling. ff14SB: improving the accuracy of protein side chain and backbone parameters from ff99SB. *Journal of chemical theory and computation.* 2015, **11**, 3696-713.

[9] W. L. Jorgensen, J. Chandrasekhar, J. D. Madura, R. W. Impey, M. L. Klein. Comparison of simple potential functions for simulating liquid water. *The Journal of chemical physics.* 1983, **79**, 926-35.

[10] Lindahl, Abraham, Hess, van der Spoel. GROMACS 2021.4 Source code. *Zenodo.* **2021**.

[11] U. Essmann, L. Perera, M. L. Berkowitz, T. Darden, H. Lee, L. G. Pedersen. A smooth particle mesh Ewald method. *The Journal of chemical physics.* 1995,**103**, 8577-93.

[12] G. Bussi, D. Donadio, M. Parrinello. Canonical sampling through velocity rescaling. *The Journal of chemical physics.* 2007, **126**, 014101.

[13] M. Parrinello, A. Rahman. Polymorphic transitions in single crystals: A new molecular dynamics method. *Journal of Applied physics.* 1981, **52**, 7182-90.